Research Square

Preprints are preliminary reports that have not undergone peer review.
They should not be considered conclusive, used to inform clinical practice,
or referenced by the media as validated information.

Smart Solar-Metal-Air Batteries Based on BiOCl Photocorrosion for Monolithic Solar Energy Conversion and Storage

Tianyi Ma (tianyima@swin.edu.au)
Swinburne University of Technology https://orcid.org/0000-0002-1042-8700
Yalin Lan
Liaoning University
Munkhbayar Batmunkh
Griffith University
Peng Li
Swinburne University of Technology
Bingzhi Qian
Liaoning University
Degang Bu
Liaoning University
Qin Zhao
Liaoning University
Hongwei Huang
China University of Geosciences Bejing
Wenping Sun
Zhejiang University
Yu Zhang
Liaoning University
Xi-Ming Song
Liaoning University
Baohua Jia
Swinburne University of Technology https://orcid.org/0000-0002-6703-477X

Article

Keywords: photocorrosion, hydrogel film electrode, solar cell, metal-air battery, BiOCl

Posted Date: August 3rd, 2021

DOI: https://doi.org/10.21203/rs.3.rs-689298/v1

License: This work is licensed under a Creative Commons Attribution 4.0 International License.
Read Full License

Smart Solar-Metal-Air Batteries Based on BiOCl Photocorrosion for Monolithic Solar Energy Conversion and Storage

Yalin Lan,[a,†] Munkhbayar Batmunkh,[b,†] Peng Li,[c] Bingzhi Qian,[a] Degang Bu,[a] Qin Zhao,[a] Hongwei Huang,[d] Wenping Sun,[e] Yu Zhang,[a,*] Tianyi Ma,[c,*] Xi-Ming Song[a,*], Baohua Jia[c,*]

[a] *Liaoning Key Laboratory for Green Synthesis and Preparative Chemistry of Advanced Materials, College of Chemistry, Liaoning University, Shenyang 110036, China*

[b] *Centre for Catalysis and Clean Energy, School of Environment and Science, Griffith University, Gold Coast, QLD 4222, Australia*

[c] *Centre for Translational Atomaterials, Swinburne University of Technology, Hawthorn, VIC 3122, Australia*

[d] *School of Materials Science and Technology, China University of Geosciences, Beijing 100083, China*

[e] *School of Materials Science and Engineering, State Key Laboratory of Clean Energy Utilization, Zhejiang University, Hangzhou, 310027, P. R. China.*

[†] *These authors contributed equally to the work.*

**Corresponding authors. E-mail: zhangy@lnu.edu.cn (Yu Zhang); tianyima@swin.edu.au (Tianyi Ma); songlab@ lnu.edu.cn (Xi-Ming Song); bjia@swin.edu.au (Baohua Jia)*

Abstract

Solar energy generation and storage are two distinct processes and integrating them in a single device is of great challenge. Herein, BiOCl hydrogel film electrode featuring excellent photocorrosion and regeneration properties acts as the anode to construct a novel type of smart Solar-Metal-Air Batteries (SMABs), which combine the characteristics of solar cell (direct photovoltaic conversion) and metal-air battery (electric energy storage and release interacting with atmosphere). The cyclic photocorrosion processes between BiOCl (Bi^{3+}) and Bi can simply be achieved by solar light illuminating and standing in dark, corresponding to the charging and discharging processes of the battery, respectively. Upon illumination, the device takes open-circuit configuration to charge itself from the sunlight. Photogenerated electrons in the conduction band of BiOCl reduce Bi^{3+} to Bi^{0} following the photocorrosion

process of BiOCl; and in the meantime, photogenerated positive charges (holes) initiate the oxygen evolution reaction to produce O_2. Notably, in this system, the converted solar energy can be stored in the SMABs without the need of external batteries to store the electricity like those for the traditional solar cells. In the discharging process in the dark, Bi^0 spontaneously turns back to Bi^{3+} producing electrons to induce oxygen reduction reaction occurring at the counter electrode (Pt/C) like metal-air battery. With an illumination of 15 min, the battery with an electrode area of 1 cm^2 can be continuously discharged for approximately 3,000 s, demonstrating a theoretical capacity of 384.75 $mAh \cdot g^{-1}$, which is higher than the theoretical capacity of lithium-ion batteries ($LiCoO_2$, 274 $mAh \cdot g^{-1}$). This novel type of SMABs is developed for the first time based on the unique photocorrosive and self-oxidation reaction of BiOCl to achieve photochemical energy generation and storage. The revealed fundamental mechanism and proposed device design create new solutions to the renewable energy harvesting and storage field. This class of solar light direct-charging battery is an effective step to fulfill the need for green and sustainable energy developments and exhibits great promise for the commercial market.

Keywords: photocorrosion, hydrogel film electrode, solar cell, metal-air battery, BiOCl

1. Introduction

Harvesting energy directly from solar energy using photovoltaic (PV) system is an ultimate solution to the ever-increasing global energy demand.[1-2] Two representative clean energy devices, namely solar cells and metal-air batteries, have drawn a great deal of attention as they promise to be the next-generation energy technologies. Intrinsically, conventional solar cells are instant photoelectric conversion devices; and the generated electric energy needs to be consumed immediately or to be stored via rechargeable batteries for later use.[3] For metal-air batteries, the large overpotential induced by sluggish reaction kinetics and insoluble discharge products usually lead to unsatisfactory battery performance.[4] Excellent efforts have been devoted to utilize photo-assisted techniques in metal-air batteries for long-term electrical storage with improved reaction kinetics and reduced overpotentials.[5] However, the charging of the photo-involved battery still requires external electricity power to a large extent, while the solar energy collection and electrical release are also two independent systems. The core of solar energy technology is to utilize solar light as an abundant energy source for continuous battery charging. Therefore, integrating these two promising energy systems into a single device as a monolithic battery for solar energy conversion and storage would be of great value.

Semiconductor catalysts with appropriate energy band positions are required to supply proper oxidation-reduction potential during the photocatalytic process.[6,7] The majority of narrow-bandgap photocatalysts with suitable band positions are unstable under illumination, such as CdS, CdSe and Cu_2O,[8a-c] due to their easy self-redox process, which is known as a photocorrosion, while photocatalysts are typically reduced using the light and cannot self-oxidize. Rarely, the photo-generated holes of photocorrosive materials such as cuprous oxide and bismuth oxide oxidize or reduce themselves under illumination.[9,10] These processes involve multiple steps of important electron transfer for energy conversion and storage using solar energy coupled with a proper fixation method,[11] although these have yet to be realized.

To this end, for the first time, we propose a new-concept of Solar-Metal-Air Batteries (SMABs), integrating the properties of solar cell and rechargeable battery. By rational electrode material design, the SMABs are expected to achieve solar energy storage and conversion through self-redox reactions. The key problem is the exploration of a recyclable valence-changed (self-corrosion) photoelectric-catalyst. The valence changes caused by the photocorrosion process can convert solar energy into chemical energy, which is then converted to electric energy by the charging process. Recently, introducing photo-assisted electrodes to restrain high charge overpotential in metal-air batteries has occasionally been reported,[12] the battery operation mechanism, however, remains to be a great challenge due to the additional charging process. In this regard, it should be significant to design a next-generation hybrid device based on self-corrosion electrode materials, which is meaningful for directly harvesting solar energy and achieving cyclic charging and discharging without an external power supply.

Herein, we discover that BiOCl exhibits the photosensitive, self-photocorrosion and regeneration properties for the novel type of SMABs. The cyclic photocorrosion processes between BiOCl (Bi^{3+}) and Bi are achieved by alternating illumination and dark standing. In order to find an efficient and scalable immobilization method of the electrode materials, calcium alginate hydrogel is adopted as an anode to construct BiOCl photocorrosion hydrogel film electrode. Such an electrode is employed for the fabrication of SMABs owing to its excellent stability and safety as well as its favorable redox potentials with Pt/O_2 as counter electrode and 0.5 M KOH as the electrolyte. Two main modes are proposed in this work, (i) 'energy storage' mode with charging and discharging separated; and (ii) 'instant energy conversion' mode. Repeated self-photocorrosion and recovery processes of BiOCl (conversion between Bi^{3+} and Bi^0) are the key to this class of SMABs developed in this work as they offer a convenient strategy to achieve charging and discharging processes driven entirely by solar energy coupled with oxygen evolution reaction (OER)/oxygen reduction

reaction (ORR) processes. We further demonstrated that the battery performance parameters, such as discharge time, can be further extended by increasing the illumination time (simulated AM 1.5 illumination), reactant content or electrode area, etc.

2. Results and Discussion

2.1 Charging and discharging mechanism in SMABs

Figure 1 schematically illustrates the basic structure and charge/discharge mechanism of the SMABs. A sandwich-like battery architecture with a BiOCl-based hydrogel film as anode, a Pt layer as cathode, and KOH solution (0.5 M) as electrolyte is presented. Specifically, in **Figure 1a**, the photoelectrons arising from the conduction band of BiOCl during illumination drive the reduction process from Bi^{3+} to Bi. Meanwhile, O_2 is released via water oxidation reaction with the assistance of photo-generated holes. In the absence of light illumination, through the discharge process, electrochemical oxidation from Bi to Bi^{3+} on the BiOCl/Bi hydrogel film occurs owing to the rather negative electrochemical potential of Bi/Bi^{3+} than O_2/H_2O. Consequently, the chemical energy is converted into electricity and the SMABs can be used to power electrical devices, as depicted in **Figure 1b**. Overall, solar energy can be stored and converted into electricity via such deliberately designed SMABs, which is achieved by light-responsive materials under illumination (charge) or non-illumination (discharge).

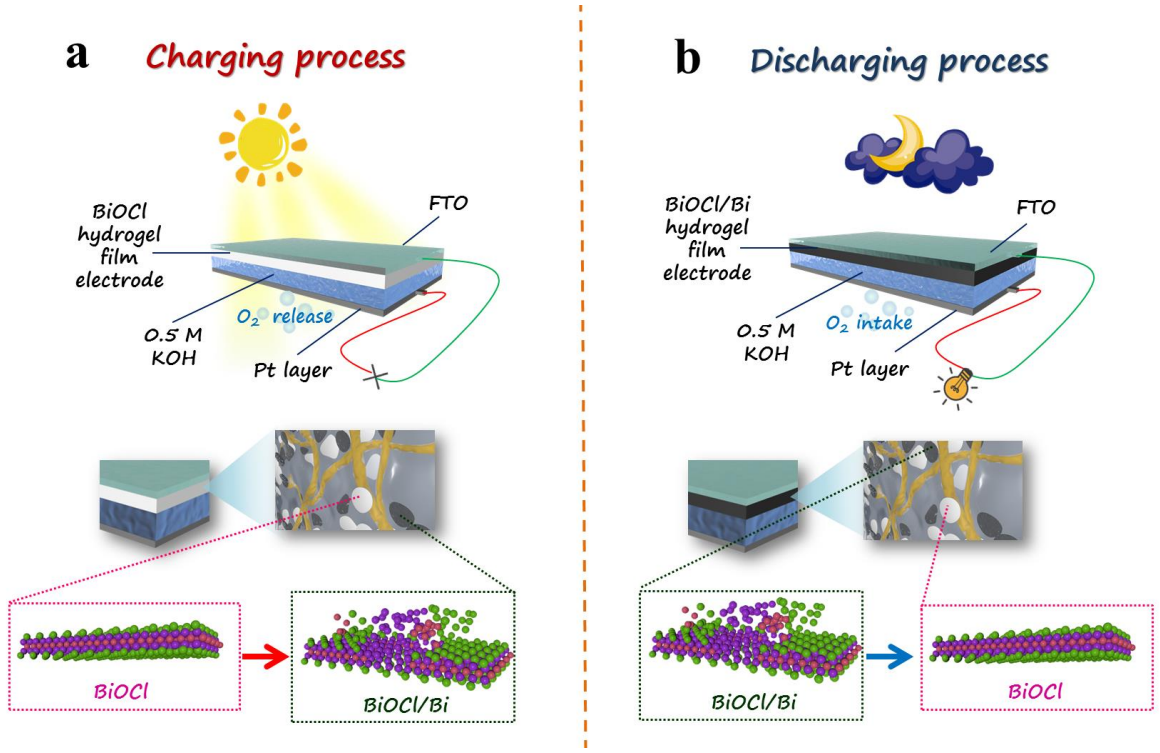

Figure 1. Schematic illustration of the (a) charge and (b) discharge mechanisms of the SMABs.

2.2 Photocorrosion gel film electrode design

The optical images of the as-prepared BiOCl hydrogel film electrode are shown in **Figure S1**. The BiOCl hydrogel film electrode is originally white, and it darkens upon illumination. The preparation process of the BiOCl hydrogel film electrode is depicted in **Figure S2**. Specifically, the hydrophilic BiOCl and sodium alginate were dispersed in water homogeneously, which was then injected into a conductive fluorine-doped tin oxide (FTO) substrate. Then the BiOCl coated FTO substrate was immersed in an aqueous solution of calcium chloride, and the gelation process was carried out for 30 min to form the calcium alginate@BiOCl hydrogel film electrode (i.e. BiOCl hydrogel film electrode),[13] in which the BiOCl are wrapped by calcium alginate hydrogel network. The hydrophilicity of BiOCl was verified by the contact angle measurement shown in **Figure S3**; and the contact angle of the BiOCl powder was 34.2~36.6°, indicating that the BiOCl is hydrophilic.

The self-photocorrosion and regeneration properties of the BiOCl were investigated using the as-prepared BiOCl hydrogel film electrode as the photo-responsive material (**Figure 2a and Figure S4**). The as-prepared white BiOCl hydrogel film on FTO substrate darkened upon illumination. The photographs of the film electrode of SMABs during discharging/charging processes are shown in **Figure S5**, demonstrating that the film darkens more with longer illumination times. Thus, we consider that the changes in the valence state of bismuth cause the color change of the film electrode.[14] It is reported that BiOCl (Bi^{3+}) and its other chemical valences (Bi^{2+}, Bi^{+}, Bi^{0}) involved compounds coexist or exist alone in the film due to the BiOCl self-photo-reduction properties.[14] It is worth mentioning that the darkened BiOCl hydrogel film electrode (after illumination for 15 min) recovers and returns to white film after standing for 12 h in the dark at room temperature (RT) (**Figure 2a**). As the pictures of the BiOCl hydrogel film electrode during the process shown in **Figure S5**, the illuminated (15 min) BiOCl (termed "BiOCl-15 min") hydrogel film electrode becomes light in color after standing for 4 h, and it turns white again after standing for 12 h, which indicates that the BiOCl exhibits the self-redox properties. Upon alternating the exposure to illumination and dark standing, the film electrode turns from black to white reversibly, suggesting a recyclable photo-responsive property of the electrode material.

The surface morphology and microscopic structure of the as-synthesized BiOCl and BiOCl hydrogel film electrode were analyzed using scanning electron microscopy (SEM) and transmission electron microscopy (TEM), as displayed in **Figure 2b-g**. The average diameter of pristine BiOCl nanosheets ranges from 200 to 500 nm.[15] More importantly, for illuminated BiOCl nanosheets, their average size is decreased to ~100-300 nm and a certain amount of BiOCl forms subsphaeroidal nanospheres, as shown in **Figure 2b**. This morphological evolution implies the photocorrosion reaction of BiOCl causing the changes in the surface chemistry. Therefore, it is also meaningful to investigate the morphology and the thickness of the BiOCl hydrogel electrode film. In **Figure 2c-d**, the BiOCl hydrogel film

electrode, featuring an average thickness of 78 μm, is composed of irregular calcium alginate gel network. The BiOCl nanosheets (highlighted by blue) sandwiched by the layers of calcium alginate hydrogel (highlighted in pink) forms a layered microstructure. After wrapping in gel network, the morphology of BiOCl nanosheets remains to be the same as before. In **Figure S6**, it can be seen that the thickness of the prepared electrode is about 1 mm before drying. The SEM image also shows that the surface of the BiOCl hydrogel film electrode is in an irregular shape, as shown in **Figure S7**. Moreover, the BiOCl particles on the surface are covered by the calcium alginate hydrogel. It was observed that Bi, O, Cl, and Ca elements are distributed evenly in the cross section of the BiOCl hydrogel film electrode by SEM elemental mapping (**Figure 2e**), which indicates the homogenous incorporation of BiOCl within the calcium alginate hydrogel. As illustrated in the TEM images of BiOCl with different magnifications (**Figure S8a**), BiOCl features disc-shape structures with a diameter of ~100-200 nm. **Figure S8b** shows the high-resolution TEM (HR-TEM) image of the BiOCl, in which a lattice spacing of 0.736 nm can be observed, corresponding to the (001) crystal plane of BiOCl. According to the TEM images in **Figure 2f**, the disc-shape BiOCl (diameter ~100-200 nm) is changed under illumination; some small particles with diameters of ~5 nm are generated on the BiOCl nanosheets. These small particles are typically observed as Bi nanoparticles,[16,17] which explains the morphology changes of the BiOCl after illumination, as observed in **Figure 2b**. The BiOCl after illumination (i.e. Bi/BiOCl heterostructure) displays two different lattice fringes with the lattice spacing of 0.736 and 0.393 nm, which can be assigned to the (001) crystal plane of BiOCl nanosheets and (003) crystal plane of the Bi nanoparticles (**Figure 2g**),[18] further confirming the existence of elemental Bi.

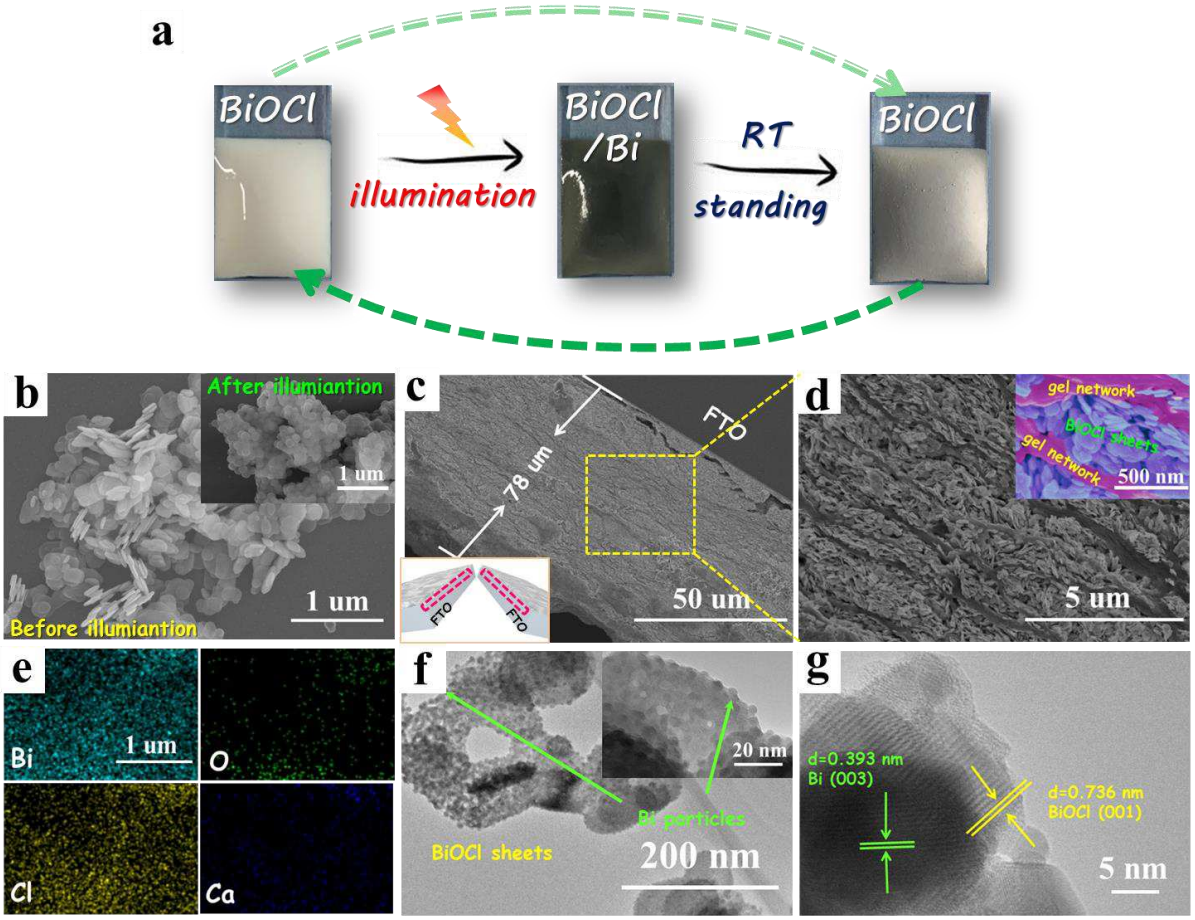

Figure 2. (a) Schematic illustration for the self-photocorrosion and recovery processes of BiOCl hydrogel film electrode; (b) SEM images of BiOCl powder. The inset image is the BiOCl after 30 min illumination; (c, d) Cross sectional SEM images of BiOCl hydrogel film electrode with different magnifications; (e) SEM elemental mapping images of BiOCl hydrogel film electrode; (f, g) TEM images of BiOCl after 30 min illumination with different magnifications.

X-ray diffraction (XRD) patterns of BiOCl and the corresponding illuminated samples are presented in **Figure 3a**, where the diffraction peaks of the as-prepared BiOCl can be well indexed to a tetragonal phase of BiOCl (JCPDS No. 73-2060).[19] After 30 min illumination, a broad peak appeared at around 22.5° (**Figure 3b** corresponds to the (003) lattice plane of a trigonal Bi (JCPDS Card No. 85-1330).[20] This result suggests that a certain amount of BiOCl is reduced and metallic Bi is formed, which is in agreement with the observed Bi NPs via TEM. The reappearance of the strong (001) diffraction peak, after standing in dark (12 h),

implies the formation of BiOCl phase as well as the reversible conversion between BiOCl/Bi and BiOCl. In order to further determine the presence of elemental Bi in the BiOCl after illumination, X-ray photoelectron spectroscopy (XPS) was conducted to characterize bonding states of the elements in the sample. The chemical compositions and elemental valence status of BiOCl were analyzed via XPS, as shown in **Figure 3c** and **Figure S9**. The binding energy (BE) and intensity of Bi 4f doublets for BiOCl (red line) and BiOCl (standing after illumination) maintain almost identical, indicating the chemical composition of BiOCl electrode can be recovered by standing 12 h after illumination. For the case of illuminated BiOCl electrode (illumination 30 min), two new shoulder peaks appeared at ~158 and ~163.8 eV can be ascribed to the metallic Bi 4f doublets (**Figure 3d**), certifying that part of metallic Bi is generated after illumination.[23] These results are consistent with the XRD results, further confirming that elemental Bi is generated in BiOCl under illumination. The O 1s spectrum of the BiOCl illuminated for 30 min is shown in **Figure S10**, which can be fitted into two peaks at binding energies of ~528.2 eV and ~530.4 for the O^{2-} and O_2^{2-} ions, respectively.[24] In **Figure S11**, two dominant peaks located at 198.2 and 200 eV can be assigned to Cl $2p_{3/2}$ and Cl $2p_{1/2}$, respectively, both of which correspond to the Cl^-.[25] XPS results of elemental Bi and O_2^{2-} ions prove that the existence of redox products caused by an illumination. The possible mechanism can be described as follows: Under illumination, the photo-generated electrons in the conduction band (CB) of the BiOCl (Bi^{3+}) reduced to Bi (Bi^0) owing to its self-reduction; and the photo-generated holes left in the valence bands (VB) oxidize O^{2-} to O_2, with possible O_2^{2-} as the intermediate during the recovery process (12 h or more standing in the dark). Due to the confinement effect of the gel film, O_2 will drive the conversion of Bi^0 to Bi^{3+} to form BiOCl.

The band structure of BiOCl was analyzed by using a ultraviolet-visible spectrophotometry (UV-vis), as shown in **Figure 3e**. The absorption edge appears at ~383 nm, and the bandgap of the BiOCl is estimated to be 3.4 eV according to the intercept of the inset plot $((\alpha h\nu)^{1/2}$ *vs.*

photoenergy) in **Figure 3e.**[16, 25] The UV-vis absorption spectroscopy of BiOCl after illumination is shown in **Figure S12**, where the presence of elemental Bi leads to a continuous absorption band in the range of 400 to 600 nm, which is in accordance with the darkened color.[26]

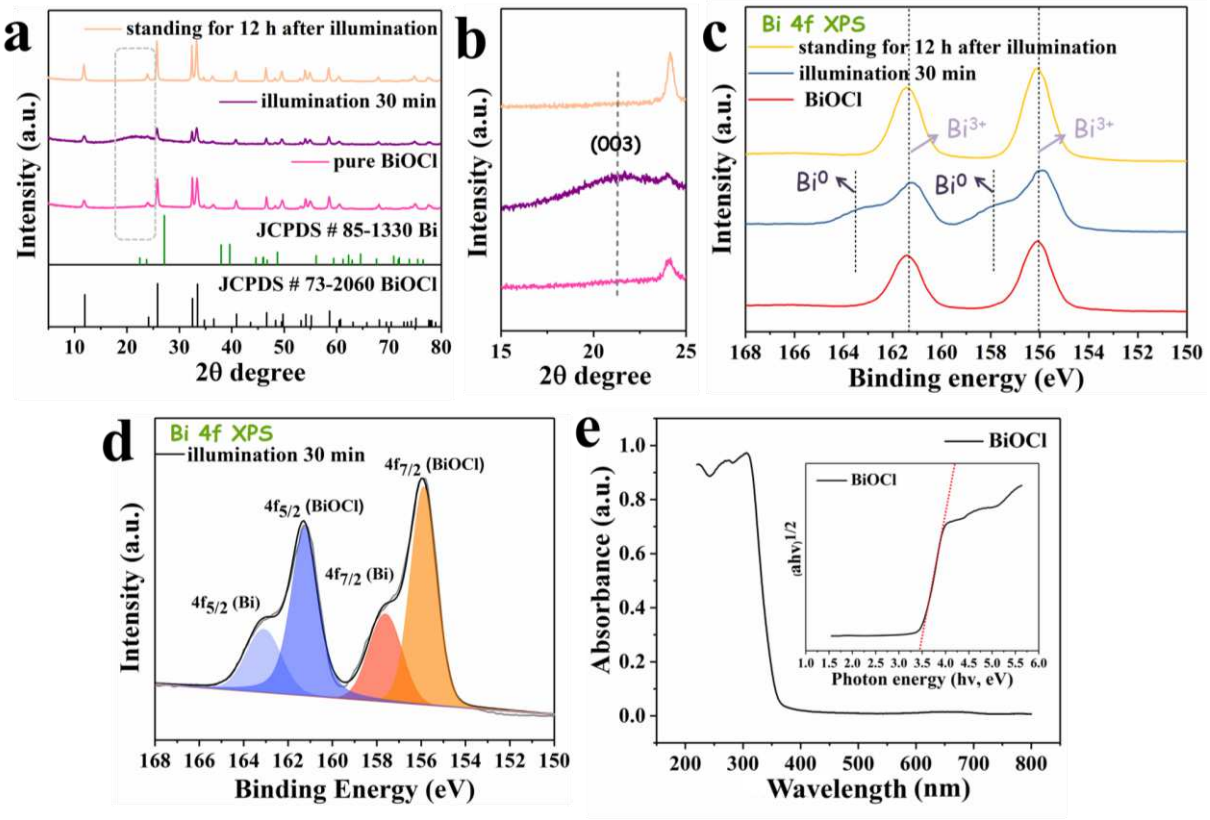

Figure 3. XRD patterns of (a) BiOCl powder, illumination for 30 min powder (BiOCl-30 min) and BiOCl-30 min standing for 12 h and (b) partial magnified details; High resolution XPS spectra of (c) Bi 4f of BiOCl powder, BiOCl-30 min and BiOCl-30 min standing for 12 h and (d) Bi 4f of BiOCl-30 min; (e) UV-vis absorption spectra of BiOCl powder (the inset is the lots of $(\alpha E)^{1/2}$ against photon energy (E) for the BiOCl, where α is the absorbance).

Metal-air batteries (MABs) generate electricity through a redox reaction between metal and oxygen.[27] In a typical discharging process, the metal anode is oxidized and releases electrons to the external circuit; oxygen accepts electrons at cathode (ORR). When the cell is charged, the process is reversed, with metal generation and oxygen evolving (OER).[28] However, some insoluble solid metal oxides or metal peroxides are generated at metal electrode during

discharging process, which reduces the rechargeability performance of the MABs.[29] Meanwhile, the air-involved electrode is also important for constructing the SMABs.

In order to establish energy band structure of the SMABs, a series of photoelectrochemical experiments were conducted. **Figure 4a** displays the Mott-Schottky plot for the BiOCl, and the positive slope of BiOCl corresponds to a n-type semiconductor in the hydrogel film electrode.[30, 31] The flat band potential of BiOCl can be approximately equal to the CB.[32, 33] The CB position of BiOCl was estimated at -1.12 eV versus Ag/AgCl electrode based on the Mott-Schottky plot. The VB level can be deduced by reducing the bandgap, and thus, the VB of BiOCl was calculated to be 2.28 eV (*vs.* Ag/AgCl) considering the band-bap of 3.4 eV. It implies that with a proper reduction potential of Bi, the photo-generated electrons in the CB can induce its self-reduction, and OER would take place, if the VB is lower than the oxidation potential of H_2O/O_2.

The ORR, OER and electrochemical properties of the BiOCl hydrogel electrode in the SMABs were evaluated in a three-electrode system with O_2-saturated 0.5 M KOH as an electrolyte, benchmark ORR catalyst Pt as a cathode, and Ag/AgCl as a reference electrode.[34] The linear sweep voltammetry (LSV) curves of the BiOCl hydrogel film electrode for OER in **Figure 4b** shows that its onset potential of OER without illumination was 0.81 V (*vs.* Ag/AgCl), and the onset potential of OER upon illumination was 0.32 V (*vs.* Ag/AgCl), indicating that the oxidation effect of the VB level of the semiconductor on H_2O was significantly enhanced by illumination due to the photo-generated holes being involved in the OER process. For the ORR with Pt electrode, the onset potential was around -0.03 V (*vs.* Ag/AgCl) as shown in **Figure 4c**, which is a typical value of conventional Pt electrode for the ORR.[35] The redox potentials of elemental Bi were identified using the cyclic voltammetry (CV) (**Figure 4d**), in which the BiOCl-30 min hydrogel film electrode was used as a positive electrode. The oxidation potential of elemental Bi was measured to be -0.45 V (*vs.* Ag/AgCl), which is more negative than the ORR potential (-0.03 V) (*vs.* Ag/AgCl). Therefore, according

to electrochemistry theory, the potential difference between Bi/BiOCl electrode and air electrode can induce the self-oxidation of Bi^0 to Bi^{3+} and ORR reaction to provide an electricity output.[36] It implies that Pt/O_2 cathode works efficiently for ORR, which is effective in constructing SMABs. Transient photovoltage (TPV) was further used to determine charge carrier diffusion properties, which performed in a self-assembling parallel-plate capacitor (**details see Experimental section in SI**).[37] As shown in **Figure 4e**, the positive response of BiOCl hydrogel film electrode corresponds to an n-type semiconductor, which is consistent with the result of Mott-Schottky test (**Figure 3e**). As illustrated in **Figure 4e**, two response peaks were observed at 2×10^{-7} s and 1×10^{-4} s. The peak located at 2×10^{-7} s represents the charge drift process of built-in electric field along the surface, while the peak at 1×10^{-4} s can be used to probe the process of charge diffusion between particles. By comparison, the process of charge diffusion of the BiOCl hydrogel film electrode lasts longer than other materials, such as $BiVO_4$, Fe_3O_4, TiO_2.[38, 39, 40] The BiOCl hydrogel film electrode obtains a significantly enhanced TPV response after illumination, indicating that the separation of photo-generated charges is promoted by the conductive elemental Bi, which is beneficial to further discharge process.

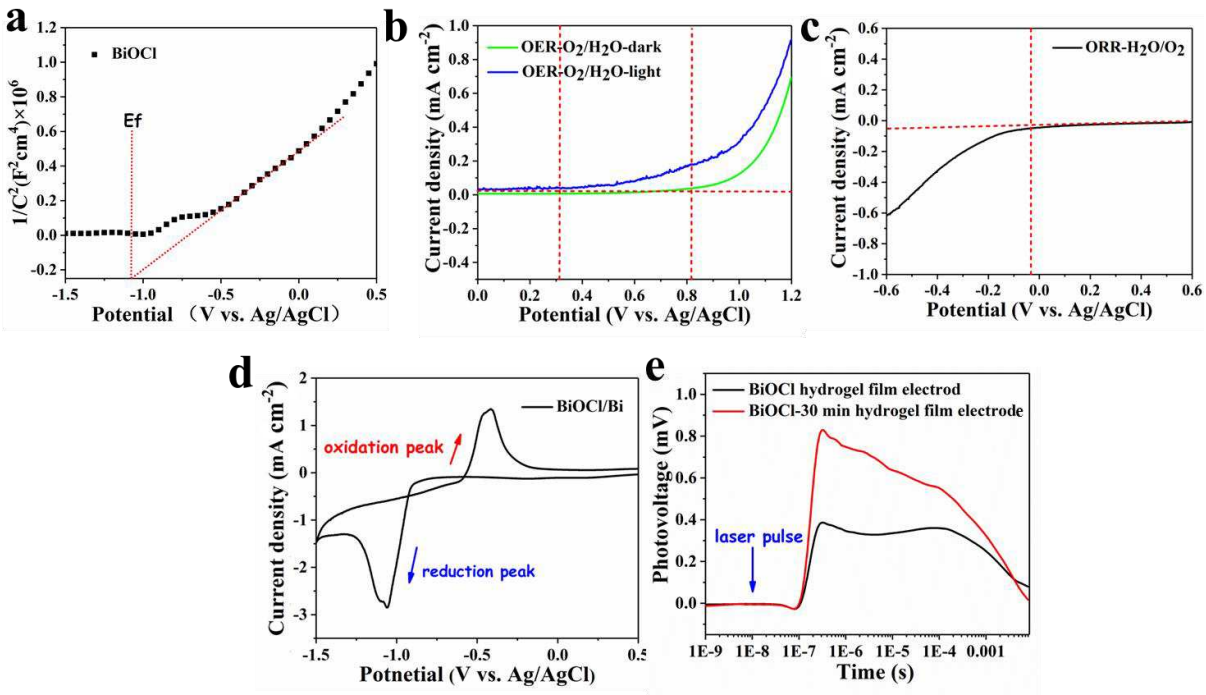

Figure 4. (a) Mott-Schottky plot for BiOCl in 0.5 M Na_2SO_4 aqueous solution (pH = 6.8); (b) OER polarization curves of BiOCl hydrogel film electrode in dark (green curve) and under illumination (blue curve); (c) ORR polarization curve of reaction with double Pt electrode; (d) Cyclic voltammogram of BiOCl-30 min hydrogel film electrode including 0.5 M KOH aqueous solution after illumination; (e) TPV of the BiOCl hydrogel film electrode before illumination (black curve) and after 30 min illumination (BiOCl-30 min, red curve) excited by 355 nm laser pulse.

2.3 Battery performance

Based on the aforementioned battery configuration, solar energy can be stored and/or converted into electricity via SMABs by using our well-designed BiOCl hydrogel film electrode. Specifically, in Figure 5, the working mode of the SMABs can be classified into "energy storage" and "instant energy conversion", where the discharge/charge process is separated and integrated, respectively. In terms of Mode one (**Figure 5a (i)**), the BiOCl hydrogel film electrode undergoes a photo-charging process when exposed to illumination for a period of time. The BiOCl is reduced by photo-generated electrons with the formation of metallic Bi, while O_2 gas is generated via water oxidation reaction induced by photo-generated holes. Upon discharge, as shown in **Figure 5a (ii)**, the metallic Bi is self-oxidized

at the anode and ORR occurs at cathode. Based on discharge/charge mode (Mode one), the proposed electrode reactions can be described as follows:

$$\text{Anode: } Bi - 3e^- + H_2O + Cl^- \rightarrow BiOCl + 2H^+$$

$$\text{Cathode: } O_2 + 4H^+ + 4e^- \rightarrow 2H_2O$$

In particular, the open circuit voltage of the BiOCl hydrogel film electrode (electrode area ~1 cm^2) increases and approaches ~0.38 V after 15 min illumination, which is close to the gap between Bi oxidation potential (-0.45 V *vs.* Ag/AgCl) and ORR potential (-0.03 *vs.* Ag/AgCl), and then further dropped to ~0.22 V (**Figure 5b**). After discharging reaction, the BiOCl hydrogel film turns white again (**Figure S5**). Upon light illumination, photo-darking immediately initiated. Our measurements examine the performance of BiOCl hydrogel film electrode at 15 min, 30 min and 60 min illuminations, and the discharge curves with different illumination times were measured (**Figure 5c)**. The rechargeability performance of the SMABs is presented in **Figure 5c**. In the first cycle (red curve), after 15 min illumination (at AM 1.5), the discharge current density gradually decreased from 3.62 to 0.43 $mA \cdot cm^{-2}$, corresponding to the oxidation reaction of elemental Bi (the color of the BiOCl hydrogel film electrode changes from dark to white). In the second cycle (blue curve), the discharge current density with 30 min illumination decreased from 3.75 to 0.63 $mA \cdot cm^{-2}$, which shows a slight improvement in the initial discharging current. In the third cycle (green curve), illumination for 60 min shows significantly improved performance in comparison with illuminations for 15 or 30 min because of its enhanced discharging current at the beginning. The discharge current density with 60 min illumination decreases from 6.24 to 0.5 $mA \cdot cm^{-2}$. These imply that the illumination on BiOCl hydrogel electrode can promote its discharge performance and significantly enhance the initial discharging current. XRD and XPS tests (**Figure 4b, c**) have already proved that the BiOCl active electrode material can be completely recovered after illumination, and these results demonstrate the good rechargeability of the SMABs. It is expected further optimization of the BiOCl hydrogel film electrode could yield better

electrochemical properties, making SMABs promising for high performance energy conversion and storage applications. The electric charge (Coulomb) during the discharge process can be calculated according to the integral formula equation (1), as shown in the Supporting information. The Coulomb of the battery (illuminated-15 min) is 1.92 C, which confirms the substantial storage of solar energy.

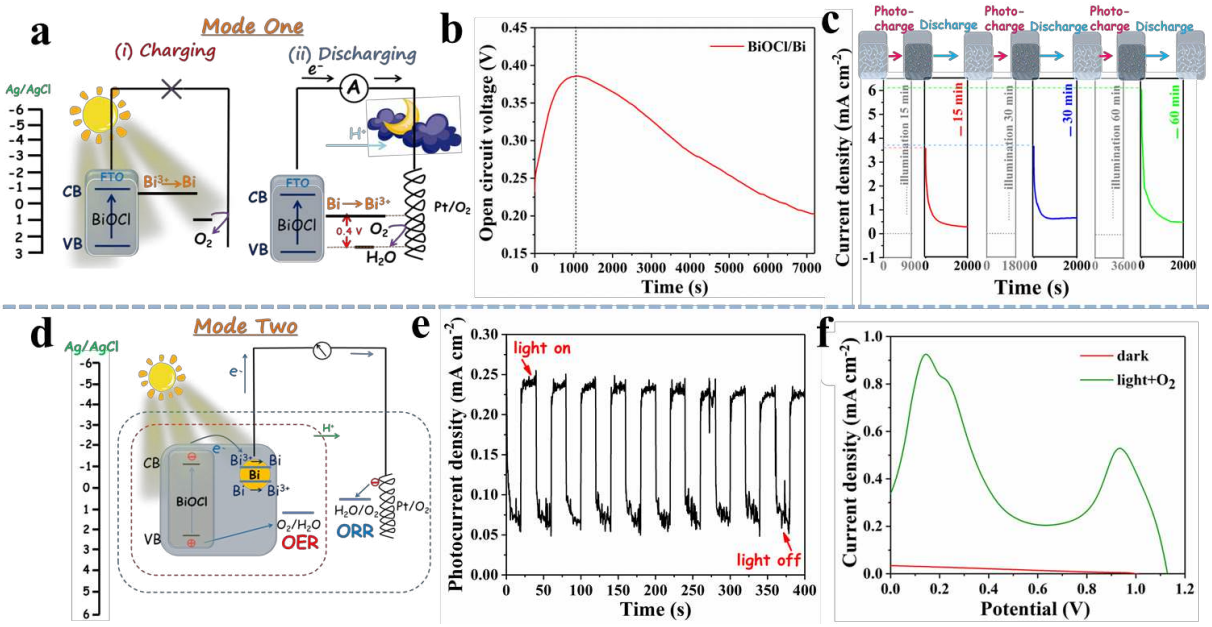

Figure 5. (a) Schematic energy level positions of Working Mode One ('energy storage') in SMABs; (b) Open circuit voltage curve of the SMABs with 15 minutes illumination in Mode One; (c) Rechargeability performance of the SMABs with different illumination times (15, 30 and 60 minutes) in Mode One; (d) Schematic energy level positions of the Working Mode Two ('instant energy conversion') in SMABs; (e) I-t characteristic curves of the BiOCl hydrogel film electrode in 0.5 M KOH aqueous solution under light with on/off cycles in Mode Two; (f) I-V characteristic curves of the SMABs based on two electrode system of BiOCl hydrogel film photoanode and Pt cathode with the electrolyte of O_2-saturated 0.5 M KOH under illumination (AM 1.5 sunlight illumination with a power density of 100 mW/cm^2) in Mode Two.

With regard to Mode Two, the "instant energy conversion" mechanism of the SMABs under real-time continuous illumination is depicted in **Figure 5d**. The position of the CB of BiOCl (-1.12 *vs.* Ag/AgCl) is a bit higher than the reduction potential of metallic Bi (-1.0 V *vs.*

Ag/AgCl). Under illumination, the photoelectrons arising from the CB of BiOCl drive the self-reduction of Bi^{3+} to Bi^0; and meanwhile, the formed metallic Bi is oxidized in air (**Figure 5a**(ii)) and generate electrons for the ORR. Furthermore, the position of the VB of BiOCl was 2.28 V *vs.* Ag/AgCl, which is more positive than the oxidation potential of H_2O versus Ag/AgCl electrode ($\varphi_{H_2O/O_2} = 0.22$ V, 0.5 M KOH); so the photo-generated holes with strong oxidation capability can enable the conversion of H_2O to O_2. Consequently**,** O_2 is produced at the anode and consumed at the cathode, forming a complete energy cycle within the SMABs. **Figure 5e** shows the I-t characteristic curve of the BiOCl hydrogel film photoelectrode. It can be seen that the SMABs show a real-time light-response, which indicates that the illuminated-BiOCl (*i.e.* BiOCl/Bi) hydrogel film electrode can generate and separate photo-induced charges. The photoelectric properties of the SMABs under dark and under AM 1.5 sunlight illumination (with O_2-bubbled) were also studied. **Figure 5f** shows the I-V characteristic curve of the battery by using traditional solar cell testing method. A two-electrode system including the BiOCl hydrogel film electrode as the working electrode and Pt electrode as the counter electrode was adopted, while a Xenon lamp (AM 1.5) was used as the light source to irradiate the BiOCl hydrogel film electrode. It is observed that when the BiOCl hydrogel film electrode is used as a photoanode and Pt/O_2 as a cathode under illumination, the short-circuit current density of the cell was 0.3 $mA \cdot cm^{-2}$ (the maximum output current density of the BiOCl hydrogel film electrode is 0.9 $mA \cdot cm^{-2}$). Unlike the typical I-V curves of traditional solar cell, two response peaks were detected for our SMABs (green line), indicating that the generated elemental Bi is involved in the charging and discharging processes. Specifically, the charging and discharging characteristics of the SMABs can be confirmed by the galvanostatic charge-discharge test as a metal-air battery, as shown in **Figure S13**. The charge-discharge curves further demonstrate that the SMABs have the charge-discharge characteristics like battery. The photovoltage of the SMABs under illumination was lower than that in the dark, which further confirms that the photo-charging

reduces the charging voltage. During the discharge process, Bi is oxidized to Bi^{3+} and gradually resumed, and the battery recyclable charging is due to the reduction process of Bi^{3+} to Bi. The BiOCl hydrogel film electrode-based SMABs were studied according to the principle of Bi-air battery, the upper theoretical limit capacity of the SMAB can reach up to 384.75 $mAh \cdot g^{-1}$ (Eq. S2), which was higher than that of the lithium ion battery ($LiCoO_2$, 274 $mAh \cdot g^{-1}$).[41] However, it should be noted that our SMABs are powered entirely by renewable solar energy without additional electric drive to meet sustainable energy needs.[42] The efficient photoelectric conversion and discharge ability of the SMABs are driven by the renewable photo-response BiOCl hydrogel electrode material. Photo-rechargeable BiOCl hydrogel film electrode can convert the chemical energy of photocorrsion products to electric energy, making it possible to construct a next generation solar energy device.

This work is dedicated to propose, for the first time, the new working principle of SMABs. Future research directions to improve the device performance would include: (1) exploiting the factors of electrode material affecting electrochemical performance (*e.g.* content, morphology, size, valence state, structure, surface area, etc.); (2) searching for suitable anode/cathode electrode materials, which are reasonable substitutes for conventional semiconductor and expensive platinum to accelerate corresponding electrochemical reaction rates, and help the electrochemical transfer of solar energy; (3) optimizing the gelation fixing strategies of photo-responsive electrode materials by building strong gel-electrode films that can adopt to extreme conditions (*e.g.* adding thermal conductive adhesion layer or creating covalent polymerization between the hydrogel and the semiconductor surfaces);[43] and (4) developing multifunctional architectures of SMABs. Air, as a general component of the battery, is involved in electrochemical reactions, which could make the battery akin to a fuel cell, with the 'fuel' being the air. It may induce the integration of the advance energy devices, and bring a positive impact on new energy policies.

3. Conclusions

In summary, a monolithic solar battery, integrating solar energy harvesting and electrical energy storage, is developed based on the unique combination of the photocorrosive and oxidation process of BiOCl semiconductors. The BiOCl hydrogel film electrode is sensitive to light illumination to allow self-oxidation and self-reduction, while its lifetimes are compatible with ORR and OER processes for the charging and discharging processes. Upon illumination, the generated photoelectrons induced by photocorrosive reaction of the BiOCl thin film electrode dedicate to the self-reduction from BiOCl to Bi and the stored chemical energy. In the discharge process, the electrons associated with self-oxidation from Bi to Bi^{3+} flow into external circuit and generate electricity output. The conceptual combination of photocorrosion with self-oxidation of low-cost BiOCl allows the creation of a new monolithic solar battery architecture. The performance can be enhanced by increasing illumination time, material content, electrode construction and others. Overall, this work introduces a dual-functional SMABs, which are powered by solar energy and recyclable materials, opening up a new pathway for utilization of solar energy and promote the development of smart controllable clean energy technologies.

4. Experimental Section/Methods

Experimental details see Supporting Information.

5. Acknowledgements

This work was supported by the National Natural Science Foundation of China (No.51773085, 52071171), the Natural Science Fund of Liaoning University (LDGY2019016), Liaoning Revitalization Talents Program - Pan Deng Scholars (XLYC1802005), Liaoning BaiQianWan Talents Program (LNBQW2018B0048), Natural Science Fund of Liaoning Province for Excellent Young Scholars (2019-YQ-04), Key Project of Scientific Research of the Education Department of Liaoning Province (LZD201902), Australia Research Council through the

Discovery Project scheme (DP190103186) and the Industrial Transformation Training Centres scheme (Grant No. IC180100005), and the Advanced Solar Facility at Swinburne University of Technology.

References

[1] M. I. Hoffert, K. Caldeira, A. K. Jain, E. F. Haites, L. D. D. Harvey, S. D. Potter, M. E. Schlesinger, S. H. Schneider, R. G. Watts, T. M. L. Wigley, D. J. Wuebbles, *Nature* 1998, *395*, 881.

[2] D. Butler, *Nature* **2008**, *454*, 558.

[3] P. Chen, G. R. Li, T. T. Li, X. P. Gao, *Adv. Sci.* **2019**, *6*, 1900620.

[4] D. Linden, T. B. Reddy, Handbook of Batteries, McGraw-Hill, New York, 3rd edn, 2002.

[5] M. Yu, X. Ren, L. Ma, Y. Wu, *Nat. Commun.* **2014**, *5*, 5111;

[6] P. J. Yang, R. R. Wang, M. Zhou, X. C. Wang, *Angew. Chem. Int. Edit.* **2018,** *130*, 8810.

[7] F. F. Wang, Q. Li, D. S. Xu, *Adv. Energy Mater.* **2017**, *7*, 1700529.

[8] (a) L. Cheng, Q. J. Xiang, Y. L. Liao, H. W. Zhang, *Energy Environ. Sci.* **2018**, *11*, 1362; (b) D. Y. Li, S. Hussain, Y. J. Wang, C. Huang, P. Li, M. Y. Wang, T. He, *Appl. Catal. B-Environ.* **2021**, *286*, 119887; (c) J. L. Liu, M. Wen, H. X. Chen, J. Li, Q.-S. Wu, *Chemplus Chem*, **2014**, *79*, 298.

[9] Q. Cai, W. T. Hong, C. Y. Jian, W. Liu, *Nano Energy* **2020**, *70*, 104485.

[10] C. Y. Toe, Z. K. Zheng, H. Wu, J. Scott, R. Amal, Y. Haung, *Angew. Chem. Int. Edit.* **2018,** *57,* 13613.

[11] S. Z. Wu, F.Zeng, H. P. Zhu, Z. Tong, *J. Am. Chem. Soc.* **2005**, *127*, 2048.

[12] D. D. Zhu, Q. C. Zhao, G. L. Fan, S. Zhao, L. B. Wang, F. J. Li, J. Chen, *Angew. Chem. Int. Edit.* **2019**, *58*, 36.

[13] X. W. Wang, H. G. Spencer, *Polymer* **1998**, *39*, 2759.

[14] S. X. Weng, B. B. Chen, L. Y. Xie, Z. Y. Zheng, P. Liu, *J. Mater. Chem. A* **2013**, *1*, 3068.

[15] Y. Ming, F. Wu, S. Banerjee, J. Park, P. Banerjee, *Chem. Commun.* **2015**, *51*, 2629.

[16] M. L. Sun, W. D. Zhang, Y. J. Sun, Y. X. Zhang, F. Dong, *Chinese J. Catal.* **2019**, *40*, 826.

[17] Y. Yu, C. Y.Cao, H. Liu, P. Li, F. F. Wei, Y. Jiang, W. G. Song, *J. Mater. Chem. A*, **2014**, *2*, 1677.

[18] W. Q. Fan, C. F. Li, H. Y. Bai, Y. Y. Zhao, B. F. Luo, Y. J. Li, Y. L. Ge, W. D. Shi, H. P. Li, *J. Mater. Chem. A*, **2017**, *5*, 4894.

[19] X. M. Mao, X. L. Li, Y. W. Wang, C. M. Fan, H. Zhang, *Chem. Eng. J.* **2014**, *247*, 241.

[20] V. L. Chandraboss, J. Kamalakkannan, S. Senthilvelan, *Appl. Surf. Sci*. **2016**, *387*, 944.

[21] X. W. Liu, H. Q. Cao, J. F. Yin, *Nano Res.* **2011***, 45*, 470.

[22] L. H. Yu, X. Y. Zhang, G. W. Li, Y. T. Cao, Y. Shao, D. Z. Li, *Appl. Catal. B-Environ.* **2016**, *187*, 301.

[23] G. Wittstoc, A. Strubing, R. Szargan, G. Werner, *J. Electroanal. Chem.* **1998***, 444*, 61.

[24] J. Hrbek, Y. W. Yang, J. A. Rodriguez, *Surf. Sci.* **1993**, *296*, 164.

[25] H. Wang, W. D. Zhang, X. W. Li, J. Y. Li, W. L. Cen, Q. Y. Li, F. Dong, *Appl. Catal. B-Environ.* **2018**, *225*, 218.

[26] L. Xu, P. C. Yan, H. N. Li, S. Y. Ling, J. X. Xia, J. X. Qiu, Q. Xu, H. M. Li, S. Q.Yuan, *Mater. Lett.* **2017**, *196*, 225.

[27] M. Zeng, Y. Liu, F. Zhao, K. Nie, N. Han, X. Wang, W. Huang, X. Song, J. Zhong and Y. Li, *Adv. Funct. Mater.* **2016**, 26, 4397.

[28] F. Y. Cheng, J. Chen, *Chem. Soc. Rev.* **2012**, *41*, 2172.

[29] L. N. Han, L. B. Lv, Q. C. Zhu, X. Wei, X. H. Li, J. S. Chen, *J. Mater. Chem. A*, **2016**, 4, 7841.

[30] D. S. Kong, *Langmuir*, **2008**, *24*, 5324.

[31] D. Chen and J. Li, *J. Phys. Chem. C*, **2010**, *114*, 10478.

[32] J. Premkumar, *Chem. Mater* **2004**, *16* ,3980.

[33] S. Iimura, H. Tezuka, A. Nakagawa, S. Yoshihara, T. Shirakashi, *Electrochemistry* **2001**, *69*, 324.

[34] B. Lim, M. Jiang, P. H. C. Camargo, E. C. Cho, J. Tao, X. Lu, Y. Zhu, Y. N. Xia, *Science* **2009**, *324*, 1302.

[35] V. A. Saveleva, V. Papaefthimiou, M. K. Daletou, W. H. Doh, C. U.-Bouillet, M. Diebold, S. Zafeiratos, E. R. Savinova, *J. Phys. Chem. C* **2016**, *120*, 15930.

[36] X. J. Li, Y. C. Tang, H. M. Lv, W. L. Wang, F. N. Mo, G. J. Liang, C. Y. Zhi, H. F. Li, *Nanoscale* **2019**, *11*, 17992.

[37] Y. Zhang, Y. Li, W. N. Sun, C. X. Yuan, B. X. Wang, W. Zhang, X.-M. Song, *Langmuir* **2017**, *33*, 12065.

[38] O. J. Sandberg, K. Tvingstedt, P. Meredith, A. Armin, *J. Phys. Chem. C* **2019**, *123*, 14261.

[39] D. Zhang, Y. M. Wang, Y. Wang, Y. Zhang, X.-M. Song, *J. Alloy. Compd*. **2020**, *815* 152377.

[40] (a) S. C. Wang, T. W. He, P. Chen, A. J. Du, K. Ostrikov, W. Huang, L. Z. Wang, *Adv. Mater.* **2020**, 32, 2001385; (b) X. H. Peng, H. B. Yu, L. Ai, N. Li, X. Wang, *Bioresource Technol.* **2013**, 144, 689; (c) S. Yang, Y. Hou, J. Xing, B. Zhang, F. Tian, X. H. Yang, H. G. Yang, *Chem-Eur J.* **2013**, 19, 9366.

[41] J. Y. Li, C. Lin, M. Weng, Y. Qiu, P. H. Chen, K. Yang, W. Y. Huang, Y. X. Hong, J. Li, M. J. Zhang, C. Dong, W. G. Zhao, Z. Xu, X. Wang, K. Xu, J. L. Sun, Feng Pan, *Nat. Nanotechnol.* **2021**, accepted.

[42] J. S. Lee, S. T. Kim, R. Cao, N. S. Choi, M. Liu, K. T. Lee, J. Cho, *Adv. Energy Mater.* **2011**, *1*, 34.

[43] S. R. Pu, J. Fu, Y. T. Liao, L. R. Ge, Y. H. Zhou, S. L. Zhang, S. L. Zhao, X. W. Liu, X. J. Hu, K. Liu, J. Chen, *Adv. Mater.* **2020**, *32*, 1907307.

The table of contents: The disc-shaped bismuth oxychloride, BiOCl, is sensitive to illumination to drive self-redox (self-photocorrosion and recovery). Smart New Solar-Metal-Air batteries (SMABs) based on BiOCl hydrogel film electrodes are assembled. The SMABs fully powered by solar energy can act as an energy storage device with the open circuit voltage of 0.38 V.

Authors: Yalin Lan,[a,†] Munkhbayar Batmunkh,[b,†] Peng Li,[c] Bingzhi Qian,[a] Degang Bu,[a] Qin Zhao,[a] Hongwei Huang,[d] Wenping Sun,[e] Yu Zhang,[a,*] Tianyi Ma,[c,*] Xi-Ming Song[a,*], Baohua Jia[c,*]

Title:
Smart Solar-Metal-Air Batteries Based on BiOCl Photocorrosion for Monolithic Solar Energy Conversion and Storage

ToC figure:

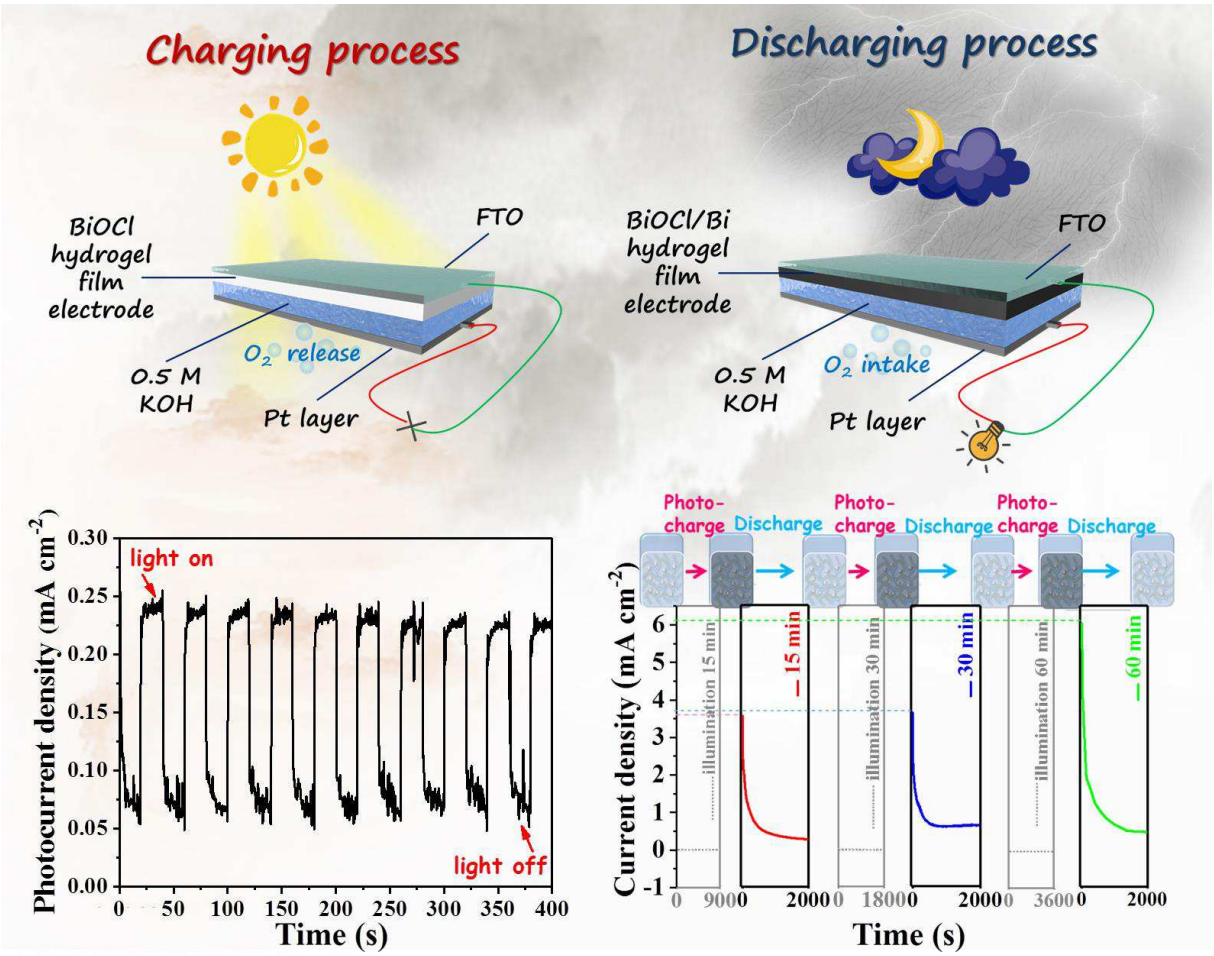

Supporting Information

Smart Solar-Metal-Air Batteries Based on BiOCl Photocorrosion for Monolithic Solar Energy Conversion and Storage

Yalin Lan,[a,†] Munkhbayar Batmunkh,[b,†] Peng Li,[c] Bingzhi Qian,[a] Degang Bu,[a] Qin Zhao,[a] Hongwei Huang,[d] Wenping Sun,[e] Yu Zhang,[a,*] Tianyi Ma,[c,*] Xi-Ming Song[a,*], Baohua Jia[c,*]

[a] *Liaoning Key Laboratory for Green Synthesis and Preparative Chemistry of Advanced Materials, College of Chemistry, Liaoning University, Shenyang 110036, China*

[b] *Centre for Catalysis and Clean Energy, School of Environment and Science, Griffith University, Gold Coast, QLD 4222, Australia*

[c] *School of Materials Science and Technology, China University of Geosciences, Beijing 100083, China*

[d] *Centre for Translational Atomaterials, Swinburne University of Technology, Hawthorn, VIC 3122, Australia*

[e] *School of Materials Science and Engineering, State Key Laboratory of Clean Energy Utilization, Zhejiang University, Hangzhou, 310027, P. R. China.*

Summary

S1. Supporting experimental section.

S2. Supporting Figure S1~S13.

Experimental section

1. Materials

The chemicals (e.g., Bismuth nitrate pentahydrate, potassium chloride, ethylene glycol, ethyl alcohol, sodium alginate, calcium chloride, etc.) used in this study were purchased from Sinopharm Chemical Reagent Co., Ltd. (Shanghai, China) without further purification and fluorine-doped tin oxide (FTO) glasses were purchased from Degussa, OPV Tech New Energy Co, Ltd. The deionized water was used in all the experiments.

2. Preparation of BiOCl

BiOCl was synthesized by a hydrolytic process according to the previous report.[1] Briefly, 2 mmol (0.9702 g) bismuth nitrate pentahydrate ($Bi(NO_3)_3 \cdot 5H_2O$) and 20 mL ethylene glycol (EG) were added into a glass beaker and sonicated for 30 min. Then, 2 mmol (0.1491 g) KCl was added to the as-prepared solution, and further sonicated for 30 min. The mixture was dropped into water, followed by stirring continuously for 12 h to get the completely precipitation. Finally, the precipitation was washed several times (water and ethanol) and dried at 55°C under oven before obtaining BiOCl powder.

3. Preparation of BiOCl hydrogel film electrode

The BiOCl hydrogel film electrode was synthesized by a simple gelation method.[2] Sodium alginate (2 g) and H_2O (98 mL) were added in a glass beaker and stirred continuously for 12 h (60°C). Subsequently, BiOCl (0.5 g) was added in sodium alginate aqueous solution (30 mL, 0.0016 g/mL) and stirred continuously for 1 h to obtain a homogeneous alginate aqueous solution. Then, the mixture (0.2 mL) was injected into the conductive fluorine-doped tin oxide (FTO) substrate. The BiOCl hydrogel film electrode was obtained after immersing the coated FTO substrates into calcium chloride aqueous solution (40 mL, 0.05 g/mL) for 30 min.

4. Materials Characterization

The XRD patterns of the as-prepared samples were conducted on a Bruker AXS D8 advanced automated diffractometer with Cu Kα radiation (λ = 1.54060 Å). X-ray photoelectron spectroscopy (XPS) was obtained using a monochromator X-rays (Quantum 2000, USA) with Al Kα radiation. The sample's morphology was observed by using a scanning electron microscope (SEM, Hitachi SU8010) and transmission electron microscopy (TEM, JEM-2100) were obtained on an apparatus. Energy-dispersive X-ray spectroscopy (EDS) and elemental mapping were acquired on the SEM (Oxford Instruments). UV-vis spectroscopy and diffuse reflectance spectroscopy (DRS) were tested on an UV-vis spectrometer (Shimadzu UV-2600) by using the semiconductor films.

5. Electrochemical characterization

The flat band (FB) potentials of BiOCl were determined from the Mott-Schottky (MS) plots recorded by electrochemistry workstation (CHI660E, Shanghai), where the sample acted as a working electrode, Ag/AgCl electrode and Pt wire electrode acted as the reference electrode and counter electrode, respectively. The OER potential was investigated in a three-electrode system in 0.5 M KOH aqueous electrolyte. The BiOCl hydrogel film electrode was used as a working electrode, the Pt wire and Ag/AgCl electrode were used as the counter and reference electrodes, respectively. The ORR potential was also tested in a three-electrode system in 0.5 M KOH aqueous electrolyte with dual Pt electrodes, and Ag/AgCl electrode were used as the reference electrodes. The redox potentials of elemental Bi in illuminated-BiOCl hydrogel film electrode were investigated in a three-electrode system in 0.5 M KOH aqueous electrolyte. The illuminated-BiOCl hydrogel film electrode was used as a working electrode, the Pt wire and Ag/AgCl electrode were used as the counter and reference electrodes, respectively. The current density-voltage (I-V) curves, photocurrent density-time (I-t), open-circuit voltage curves, cycling discharge curves and constant current charging-discharging were tested in a two-electrode system including the BiOCl hydrogel film

electrode as the working electrode, the Pt/O_2 as the counter electrode and 0.5 M KOH aqueous solution as the electrolyte. A BiOCl hydrogel film on the FTO substrate, a piece of 10 μm-thick mica and a platinum wire gauze electrode were assembled to make up the sample-chamber-like parallel-plate capacitor. A laser pulse (355 nm, 50 $mJ \cdot cm^{-2}$) with a width of 10 ns was used to excite the sample, and the photovoltaic signal was recorded over 100 ns to 10 ms.

The Cullen number (C) is calculated according to the Eq. S1 below:

$$C = \int_{t_0}^{t_d} f(I \times V) dt_d \quad (1)$$

Where C is the Cullen number, V, I, t_d, t_0 are open circuit voltage, short circuit current, discharge time and initial discharge time, respectively.

The theoretical capacity ($mAh \cdot g^{-1}$) of the Solar-Metal-Air is calculated according to the Eq. S2 below:

$$Theoretical\ Capacity = \frac{\frac{1g}{M_{Bi}} \times F \times 3}{1\ mAh}$$

$$1\text{mAh} = 3.6\ \text{C} \quad (2)$$

Here, M_{Bi} is the molecular mass of elemental Bi, F is the Faraday constant (96485 $C \cdot mol^{-1}$).

Supporting Figures

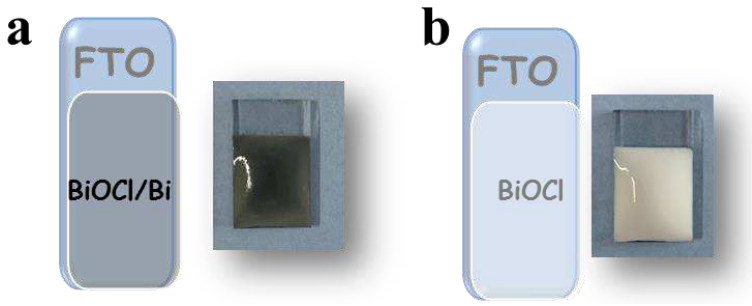

Figure S1. Photographs of the electrodes after (a) charging and (b) discharging process in SMABs.

Figure S1a shows the BiOCl/Bi hydrogel film electrode in the Solar-Metal-Air battery, it can be clearly seen that the electrode is black in the process of discharging, which is prepared by BiOCl hydrogel film electrode in solar-light-illumination (15 min or more), furthermore, with the discharging time goes on, the BiOCl/Bi film electrode will gradually become white. The BiOCl hydrogel film electrode is illustrated in Figure S1b, initially, the BiOCl film electrode is white, as the light time increases, and the color of the film electrode gradually turns black.

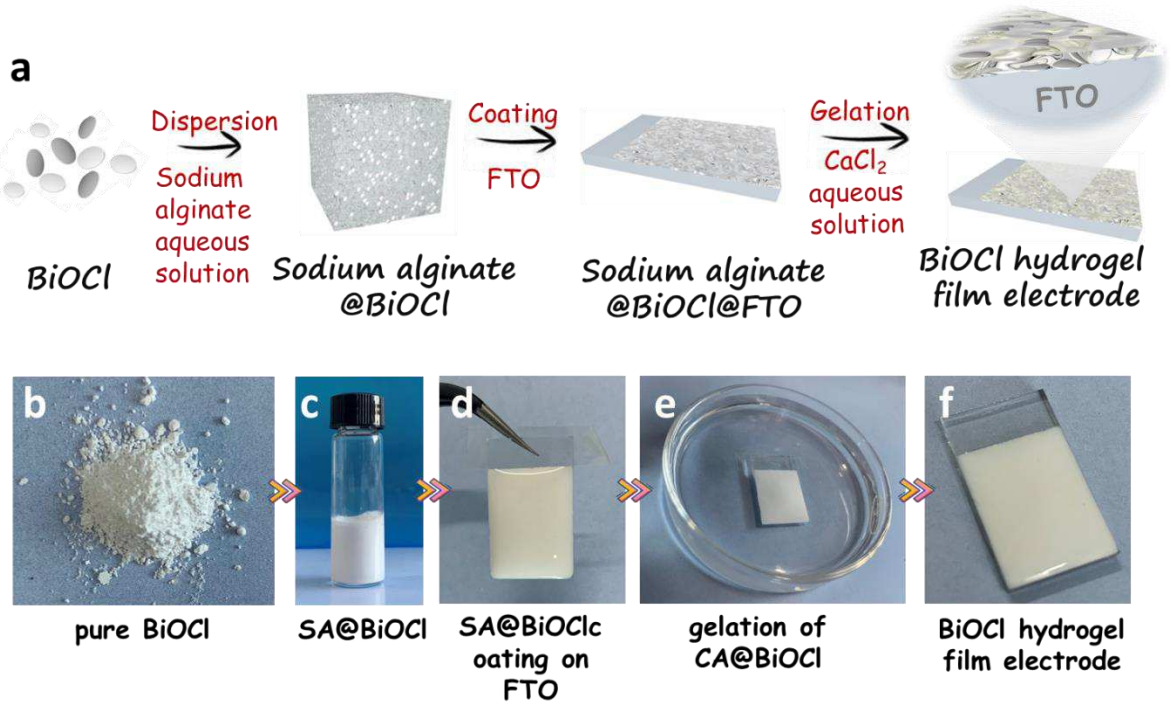

Figure S2. (a) Schematic illustration of the synthesis process of BiOCl hydrogel film electrode and photographs of the preparation process: (b) BiOCl powder; (c) the mixture of sodium alginate@BiOCl in a vial; (d) the FTO with sodium alginate@BiOCl coatings; (e) the gelation process of calcium alginate@BiOCl; (f) the BiOCl hydrogel film electrode.

BiOCl particles and sodium alginate are dispersed in water together, and the mixture of sodium alginate@BiOCl was extruded from a syringe onto the conductive fluorine-doped tin oxide (FTO) substrate. Then the sodium alginate@BiOCl coated FTO substrate was immersed in a calcium chloride aqueous solution (30 min or more) to form the calcium alginate@BiOCl hydrogel film electrode (i.e. BiOCl hydrogel film electrode).

Figure S3. Contact angle of BiOCl powder.

As shown in Figure S3, the contact angle of BiOCl powder is 34.2~36.6°, suggesting that BiOCl is hydrophilic and easy to dissolve in water or water solution.

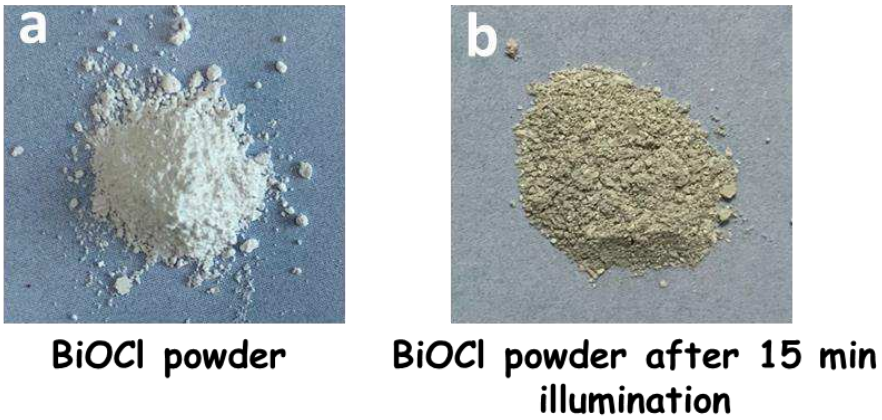

Figure S4. Photograph of (a) BiOCl powder and (b) BiOCl-15 min powder.

.

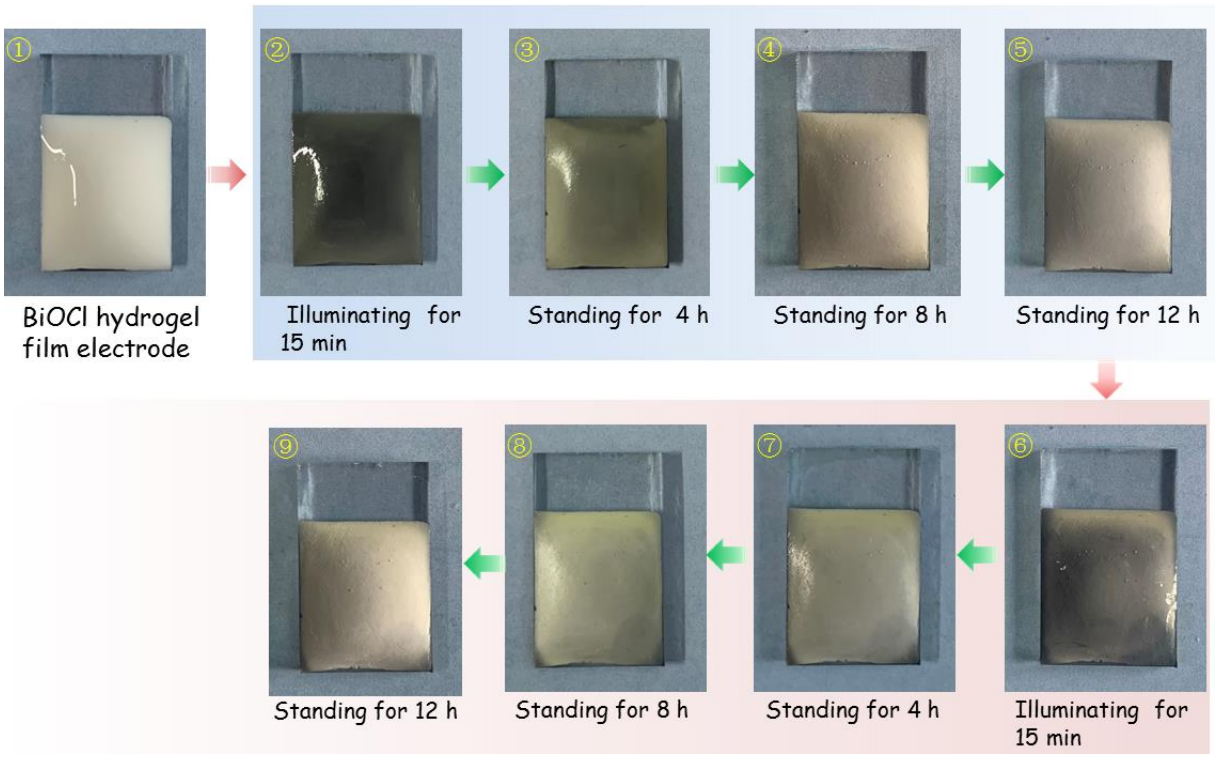

Figure S5. Photograph of the BiOCl hydrogel film electrode during the self-photocorrosion process.

The self-corrosion (self-redox) processes are shown in Figure S5, in two cycles, the BiOCl-15 min film electrode becomes light in color after standing 4 h, and it turns completely white after standing 12 h, these results prove that the self-corrosion (self-redox) processes are cyclic.

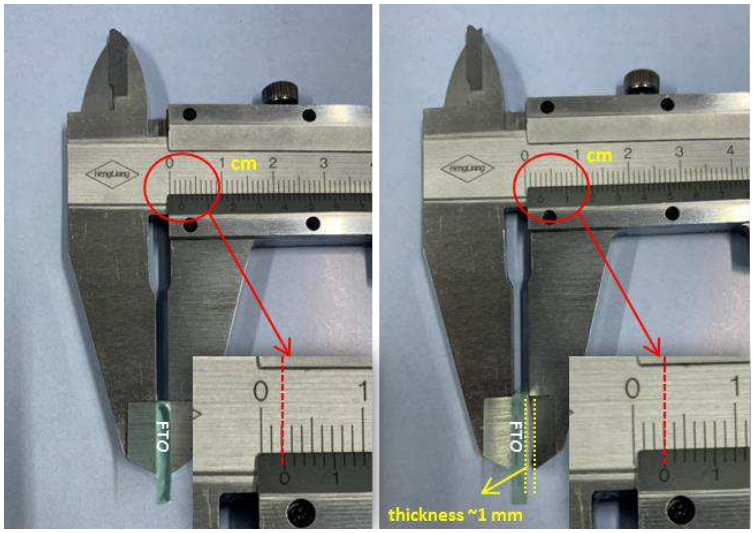

Figure S6. Photograph of the thickness of BiOCl hydrogel film electrode.

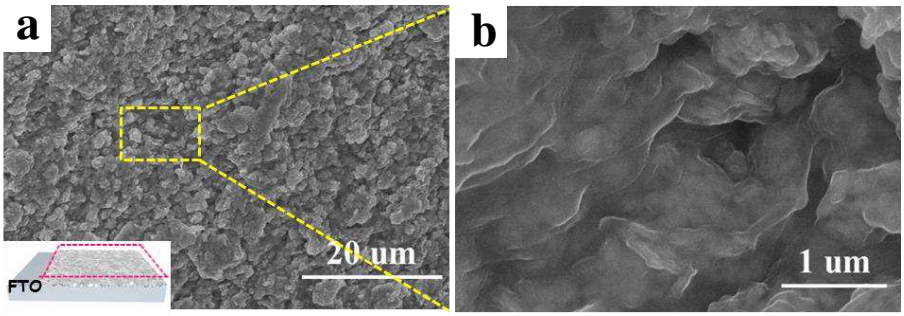

Figure S7. SEM images of surface morphology of the BiOCl hydrogel film electrode with different magnification.

As shown in Figure S7a, the surface of the BiOCl hydrogel electrode film exhibits a rough geometric squares structure. Moreover, the BiOCl particles on the surface are covered by calcium alginate hydrogel (Figure S7b).

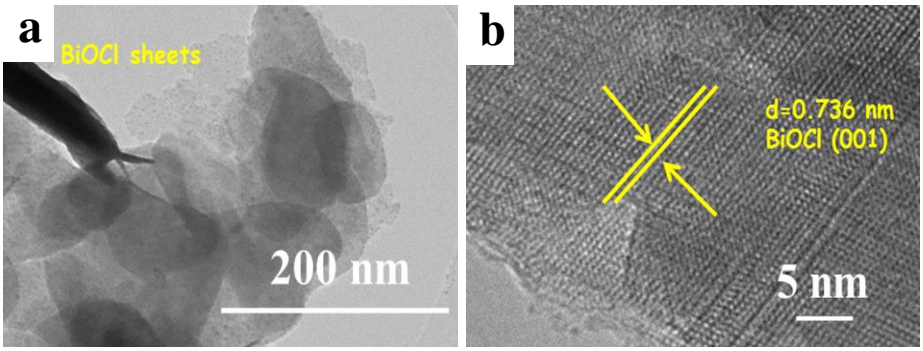

Figure S8. TEM images of BiOCl with different magnification.

Figure S8a shows the TEM image of the BiOCl, and it can be clearly seen that the BiOCl with disc-shape structures exhibits a diameter of ~100-200 nm. Figure S8b shows the HR-TEM image of the BiOCl, with a lattice spacing (0.736 nm) can be observed, which corresponding to the (001) crystal plane of BiOCl.

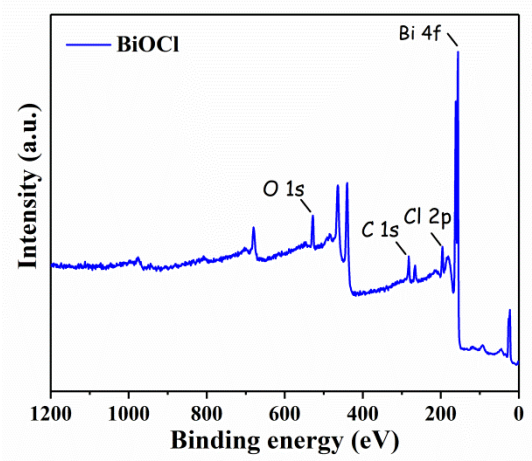

Figure S9. XPS survey spectra of BiOCl.

Figure S9 shows that BiOCl contains Bi, O, C and Cl elements. Among them, C 1s is chosen as the reference line.[3]

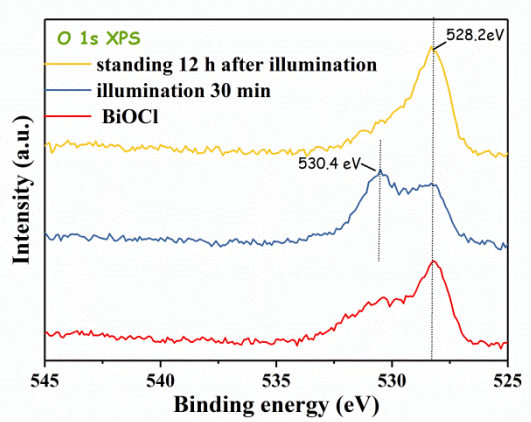

Figure S10. XPS O 1s spectra of the BiOCl-30 min powder.

Figure S10 shows the O 1s spectrum of the BiOCl-30 min powder, which can be fitted with two main peaks at binding energies of ~528.2 eV and ~530.4 for the O^{2-} and O_2^{2-} ions, respectively.[4]

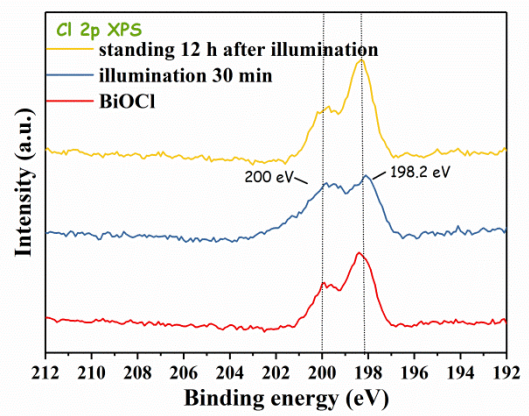

Figure S11. XPS Cl 2p spectra of the BiOCl-30 min powder.

In Figure S11, two dominant peaks located at 198.2 eV and 200 eV can be assigned to Cl $2p_{3/2}$ and Cl $2p_{1/2}$, respectively, which are all correspond to the Cl^-.[3]

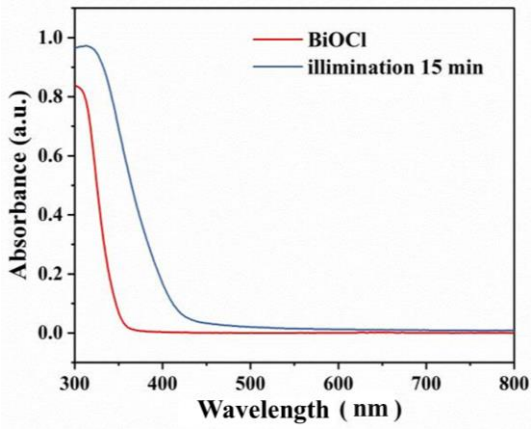

Figure S12.UV-vis absorption spectra of BiOCl powder and BiOCl-15 min powder.

Figure S12 shows the UV-vis absorption spectra of BiOCl and BiOCl after 15 min illumination. It can be clearly observed that the BiOCl present an absorption edge at about 370 nm, indicating that BiOCl mainly absorb UV light. Compared with BiOCl, the absorption region of the BiOCl-15 min powder (i.e. BiOCl/Bi) was broadened to ~600 nm. It proves the existence of Bi, and Bi contributes to improving the utilization ratio of light.

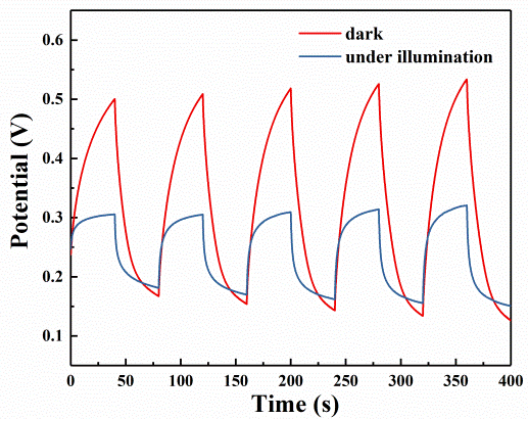

Figure S13. Cycling performance of the SMABs in the dark and under illumination at current density of 0.01 mA·cm^{-2}.

The charge-discharge curves of the SMABs before and after illumination are shown in Figure S13, which further confirm that the light-charging reduces the charging voltage of the SMABs.

References

[1] Y. Myung, F. Wu, S. Banerjee, J. Park, P. Banerjee, *Chem. Commun.* **2015**, *51*, 2629.

[2] K. Liu, H. J. Ding, J. Liu, Y.Chen, X. Z. Zhao, *Langmuir* **2006**, *22*, 9453.

[3] H. Wang, W. D. Zhang, X. W. Li, J. Y. Li, W. L. Cen, Q. Y. Li, F. Dong, *Appl. Catal. B-Environ.* **2018**, *225*, 218.

[4] J. Hrbek, Y. W. Yang, J. A. Rodriguez, *Surf. Sci.* **1993**, *296*, 164.